

# THE EFFECT OF MULTI-AXIAL RESTRAINT ON ASR-AFFECTED CONCRETE

Cyrille F. Dunant\*, Evan C. Bentz

University of Toronto, Department of Civil Engineering,  
Galbraith building, 35 St. George st., M5S 1A4 Toronto, Canada

## Abstract

ASR is the most common cause for concrete degradation not related to reinforcement bars. In laboratory conditions, the most common test procedure for ASR is the measure of the macroscopic free expansion of samples. This expansion however is the result of both the alkali-silica reaction and the mechanical effects stemming from the swelling of the resulting gel pockets. In structures, the concrete is typically under complex loading conditions. Prediction of the evolution of the material properties in relation to the externally applied loads is crucial to schedule the repairs and eventual replacement of the affected structures

Previous studies [2, 6] have shown both the dramatic effect of uniaxial stress on the recorded expansion, and an important effect in the case of radial restrained expansion [5]. An experimental setup where reinforced samples are subject to different levels of restraint on each axis was built. The non-linear response of the samples is modelled using simulated microstructures. The results highlight the importance of fracture mechanics at the microstructural scale and help further the understanding of ASR as a coupled chemical-fracture mechanics phenomenon.

**KEYWORDS:** anisotropy; modelling; restraint; microstructure; testing

## 1 INTRODUCTION

ASR is a common cause of concrete degradation, in particular in mass concrete structures. For logistical reasons, such structures can only be built with aggregates available near the construction site. Many such structures were constructed before the risk posed by ASR was recognised and were built with reactive aggregates. As ASR is a slow reaction, these structures can have a long useful life span if repairs can be scheduled and the evolution of the reaction predicted.

Although ASR is a chemical reaction which dissolves amorphous silica in the aggregates and precipitates an expansive gel, its consequences are mechanical: material degradation, development of internal loads.

---

\*Correspondence to [cyrille.dunant@gmail.com](mailto:cyrille.dunant@gmail.com)

The expansion measured macroscopically is due to the formation of amicro-crack network at the level of the aggregates and the paste. The formation of such networks of cracks can be altered by the external loading of the material. Cracks tend to form in the direction normal to the principal tensile stress. This induces anisotropy in the expansion, and in the mechanical properties of the material.

The location of the gel and the morphology of the crack network depend on the mineralogical nature of the aggregates. Two broad classes of aggregates have been identified: the slow-reacting aggregates and the fast reacting aggregates [7]. The slow-reacting aggregates are characterised by the formation of gel pockets dispersed throughout their volume. This causes the formation of cracks within the aggregates, which only enter the cement paste during the later stages of the reaction. The fast-reacting aggregates are more homogeneously reactive, and react more markedly on their surface. This causes cracks to appear in the cement paste early in the development of the reaction, leading to more extensive damage and faster expansion.

The study of the effect of the loading condition on the development of the effects of ASR is complicated by the anisotropy of the expansion. It has been reported by Smaoui and colleagues [8] that the expansion in the direction of the casting is larger than in the directions orthogonal to it. This effect has not been explained and is probably intrinsic to the casting process. In their studies, Multon and colleagues and Berra and colleagues [6, 2] both restrained the expansion of cylindrical samples using steel or fibres. They found that the expansion is partly redistributed along the less restrained direction. However, the measure of this redistribution could be affected by the anisotropy of the reaction. To understand the relative change in expansion as a function of restraint, an understanding of the micro-mechanical effects of the reaction is necessary. Numerical models are ideally suited to such studies.

Modelling of ASR at the micro-structure level has proved to be a valuable approach to understand the mechanisms which link the reaction to its consequences. Notably, finite element analysis on explicitly modelled concretes and mortars was used to link the damage morphology at the micro-structure level and macroscopic expansion [4]. This approach showed that the location of the gel was critical to explain the loss of material properties, stiffness and strength, observed experimentally.

This paper presents a combined experimental and numerical setup designed to capture the effect of tri-axial restraint states on ASR-affected samples. In the experiments presented here, only two axes are restrained, but the amount of restraint is different in all three axes. A schematic comparison of the setups used in this study and in the literature can be seen on Figure 2.

## 2 MATERIALS AND METHODS

To cast the concrete used in this study, Sudbury aggregates, were crushed and sieved to form 0-2 mm, 2-4 mm, 4-8 mm, 8-12 mm and 12-16 mm fractions which were then composed to form a continuously graded particle size distribution (Figure 1). A single batch of concrete was mixed to prepare all the samples.

The mix was prepared using a water/cement ratio of 0.52 and the viscosity was controlled by the addition of both superplasticizer and viscosity-modifying admixtures. The samples were filled in two layers and vibrated after each layer was placed.

Each sample is contained in a restraining mould. This mould is composed of independent steel plates,

connected in pairs by threaded rods (Figure 2). To maintain the moulds in place during casting, a wooden scaffolding was constructed. The choice of the diameter of the threaded rods made it possible to vary the restraint ratio on each sample. Sixteen restraint conditions are tested (Table 1). The conditions cover practically relevant amounts of reinforcement, ranging from 1 to 3%.

All samples were demoulded at 24 hours, and put into a fog room for 28 days. At 28 days, the initial samples sizes were measured and the samples were immersed into 250 mmol/ℓ solutions of sodium hydroxide and placed into a temperature-controlled room kept at 38 . The concentration of the alkalies in the curing bath is meant to be similar to that of the cement pore solution and thus prevent leaching.

Expansion measurements were performed on average every 21 days. Before each measure, the samples in solution were removed from the hot room and placed to cool at 20 . After 24 hours of cool-down, they were individually removed from their solution, wiped and measured.

## 2.1 Numerical modelling

Numerical modelling was performed using the AMIE simulation framework [4]. Aggregates following the prescribed particle size distribution are generated and placed randomly in a 2D slice. Both the size distribution and the aggregate fraction are accurately represented. Once the simulated geometry has been generated, it is meshed. Gel pockets are then nucleated randomly in the aggregates. The ASR model used in this study was originally based on back-scattered electron microscopy observations on polished sections. It was observed (Figure 3) that in slowly-reacting aggregates the reaction occurs in localised gel pockets, found throughout the aggregates [1]. A numerical tool was implemented to generate equivalent 2D micro-structures, mesh them and perform non-linear finite element analysis on them [3].

As the gel pockets are much smaller than the aggregates, it is not practical to mesh them explicitly. Thus, they are represented using extended finite elements, which model the interface between the gel and the aggregate as a material discontinuity. The gel pockets are then made to expand by imposing an applied strain. This numerical method has the added advantage that it does not require re-meshing.

To model the restraint, blocks of material are placed around the simulated sample. The stiffness of these blocks is adjusted to be the same as that of the threaded rods in the experimental samples. This was preferred to explicitly modelling rods which would have disturbed the stress and strain fields in the 2D simulations more than they do in the experiments (Figure 4).

In the following descriptions, the stress  $\boldsymbol{\sigma}$  and strain  $\boldsymbol{\epsilon}$  are formulated as vectors:

$$\boldsymbol{\epsilon} = \{\epsilon_x, \epsilon_y, \gamma_{xy}\}^T \quad (1)$$

$$\boldsymbol{\sigma} = \{\sigma_x, \sigma_y, \tau_x\}^T \quad (2)$$

And the derivation operator  $\nabla$  is:

$$\nabla = \begin{pmatrix} \partial/\partial x & 0 \\ 0 & \partial/\partial y \\ \partial/\partial y & \partial/\partial x \end{pmatrix} \quad (3)$$

**Constitutive relations** The matrix and aggregate are modelled as linear elastic damaging materials. Their behaviour is simple as it is assumed that the complexity of the observed macroscopic behaviour lies in the geometric make-up of the problem. The constitutive relationship are ( $\mathbb{C}_{\text{matrix}}$  the Cauchy-Green Stress tensor,  $d$  the damage parameter):

$$\boldsymbol{\sigma} = \mathbb{C}_{\text{matrix}}(1 - d)\boldsymbol{\epsilon} \quad (4)$$

The equivalent stress is kept constant, independent of the damage state of the material, and is calculated as ( $\sigma_i$  the  $i^{\text{th}}$  principal stress):

$$\sigma_{\text{eq}} = \max_{i=1,2,3} \sigma_i \quad (5)$$

The limit stress is considered reached when (Figure 6):

1. at the point considered,  $\sigma_{\text{eq}} \geq \sigma_{\text{crit}}$
2. the point considered is at a distance less than  $\delta$  of the maximum  $\sigma_{\text{eq}}$  in its neighbourhood
3. A volume  $\frac{4}{3}\pi\delta^3$  has  $\sigma_{\text{eq}} \geq \sigma_{\text{crit}}$  (in 2D a surface of area  $\pi\delta^2$ )

The criterion used in the simulation is the comparison between the principal stress in the element and a threshold. Further, the damage density per unit volume is limited so the elements can only dissipate finite amounts of energy while they are damaged.

The gel pockets are simply linear elastic. Further, strains are imposed which simulate the expansion. The force imposed is:

$$\mathbf{f} = \nabla \cdot (\mathbb{C}_{\text{gel}} \boldsymbol{\epsilon}_{\text{imposed}}) \quad (6)$$

This same method is used to impose shrinkage strain on the paste.

**Boundary conditions** Three set of boundary conditions are considered in the simulations, reflecting those of the experiments. In the first case, the samples are free to expand, and all boundaries are free. In the second, a single axis is restrained, and the concrete of the simulation is placed between two plates of varying stiffness. Finally, when two axes are restrained, the concrete in the simulation is placed between four plates (Figure 5).

**Weak form based on the weighted residual Bubnov-Galerkin method** For the finite element implementation, the test and trial functions are chosen in the same space. triangular finite elements were used. The shape functions in the linear archetypal elements are:  $h = \{\xi, \eta, 1 - \xi - \eta\}$ .

All behaviour laws are expressed in the archetypal element and the projection to the actual elements is done by the integration scheme. In the implementation, the weak form is expressed per couple of degrees

of freedom in each element  $e$ :

$$\mathbf{B}_{ij} = \int_e \nabla b_i^T \mathbb{C} \nabla b_j \, de \quad (7)$$

Further, for the gel and shrinking paste, the following extra forces are applied:

$$\mathbf{f}_i = \int_e \nabla b_i^T \mathbb{C} \boldsymbol{\epsilon}_{\text{imposed}} \, de \quad (8)$$

As extended finite elements are used for the simulation of the hard interface between the matrix and the gel, supplementary shape functions need to be added to the relevant elements. As the inclusions are assumed to have a spherical shape, with radius  $r$  and centre  $\mathbf{c}$ , the supplementary shape functions  $\tilde{h}_i$  attached to the degrees of freedom of node  $\mathbf{u}_i$  are simply:

$$\tilde{h}_i = \{b_i(|\text{dist}(\mathbf{x}, \mathbf{c}) - r| - |\text{dist}(\mathbf{u}_i, \mathbf{c}) - r|)\} \quad i = 1, 2, 3 \quad (9)$$

This form allows the displacements of the nodes to be obtained without further post-processing, as the contribution of the enrichment shape functions is 0 at these points.

### 3 RESULTS AND DISCUSSION

The samples exhibited shrinkage for the first 150 days of their immersion. The observed shrinkage value is consistent with the expectation for this concrete. As the expansion is obtained by measuring the distance between facing plates, the measurements during this period are noisy: the concrete is receding from the plates. The observed shrinkage however, demonstrates that the bond between the rods and the concrete is good: the plates are touching the concrete, but are attached only to the rods. Once the expansion had started again, the noise of the measure diminished dramatically. This is explained by the fact that the concrete pushing on the steel plates stabilises the measure (Figure 7). In this figure, the strains have been set at 0 at onset of the expansion.

To reproduce the shrinkage which was observed in the experiments, an imposed negative strain (-1500  $\mu\text{m}/\text{m}$ ) was applied to the paste of the simulated microstructures. This strain was fit to simulate the observed shrinkage of the samples. The simulated macroscopic expansions come from the interaction between the shrinking paste, the expanding gel pockets and the stiff aggregates. Good agreement between the experiments and the simulations validates the geometrical representation of the concrete (Figure 8).

The recorded expansions at the time of writing this paper are very small. Indeed, the corresponding simulated expansions are still within the elastic range. As the expansions develop, the difference between the simulated elastic values and the experiments should increase. The experiments will then be compared to non-linear simulations, using the same numerical setup. The lateral expansion results have more noise than the longitudinal ones. This is explained by the measuring procedure: the lateral expansion is measured at four points on each sample, whereas the longitudinal expansion is only taken at two points, thus the dispersion in the lateral measures is approximately half that of the longitudinal.

A crucial point of this experimental setup is that any anisotropy observed should come only from the interactions between the reaction and the imposed restraint. To assess this, we have compared the difference in expansion along the two axes with the equivalent elastic predictions (Figure 9). In the model, the expansion concrete is isotropic to within 1%. The good agreement observed between the model and the prediction shows that ASR expand similarly in all directions normal to the direction of casting.

#### 4 CONCLUSION AND PERSPECTIVES

In this paper, a coupled experimental and simulation study of ASR-reactive samples under restraint has been presented. The microstructural model was shown to be in good agreement with the experimental observations. The preliminary results presented validate the experimental set-up as well as the numerical analysis. The good agreement between elastic simulations the experiments indicate that at this early stage of the reaction, no significant damage was caused. As the monitoring of the experiments continue, non-linear effects are expected.

#### References

- [1] M. Ben Haha, E. Gallucci, A. Guidoum, and K. L. Scrivener. Relation of expansion due to alkali silica reaction to the degree of reaction measured by sem image analysis. *Cem. Concr. Res.*, 37(8):1206–1214, August 2007.
- [2] M. Berra, G. Faggiani, T. Mangialardi, and A. E. Paolini. Influence of stress restraint on the expansive behaviour of concrete affected by alkali-silica reaction. *Cem. Concr. Res.*, 40:1403–1409, 5 2010.
- [3] C. Dunant, P. N. Vinh, M. Belgasmia, S. Bordas, and A. Guidoum. Architecture tradeoffs of integrating a mesh generator to partition of unity enriched object-oriented finite element software. *Revue Européenne de Mécanique Numérique*, 16:237–258, March 2007.
- [4] C. F. Dunant and K. L. Scrivener. Micro-mechanical modelling of alkali-silica-reaction—induced degradation using the amie framework. *Cem. Concr. Res.*, (4):517–525, 4 2010.
- [5] M. Kawamura and K. Iwahori. Asr gel composition and expansive pressure in mortars under restraint. *Cem. Concr. Compos.*, 26(1):47 – 56, 2004.
- [6] S. Multon and F. Toutlemonde. Effect of applied stresses on alkali-silica reaction-induced expansions. *Cem. Concr. Res.*, 36(5):912–920, 2006.
- [7] J. M. Ponce and O. R. Batic. Different manifestations of the alkali-silica reaction in concrete according to the reaction kinetics of the reactive aggregate. *Cem. Concr. Res.*, 36(6):1148–1156, 2006.
- [8] N. Smaoui, M.-A. Bérubé, B. Fournier, and B. Bissonnette. Influence of specimen geometry, orientation of casting plane, and mode of concrete consolidation on expansion due to ASR. *Cem., Concr., Aggregates*, 26(2):1–13, 2004.

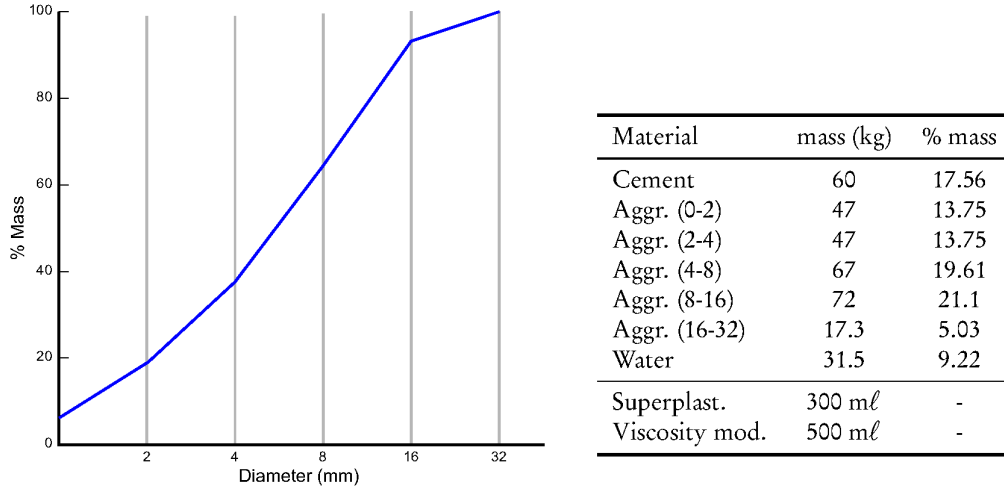


Figure 1: Particle size distribution of the aggregates used in the experiments.

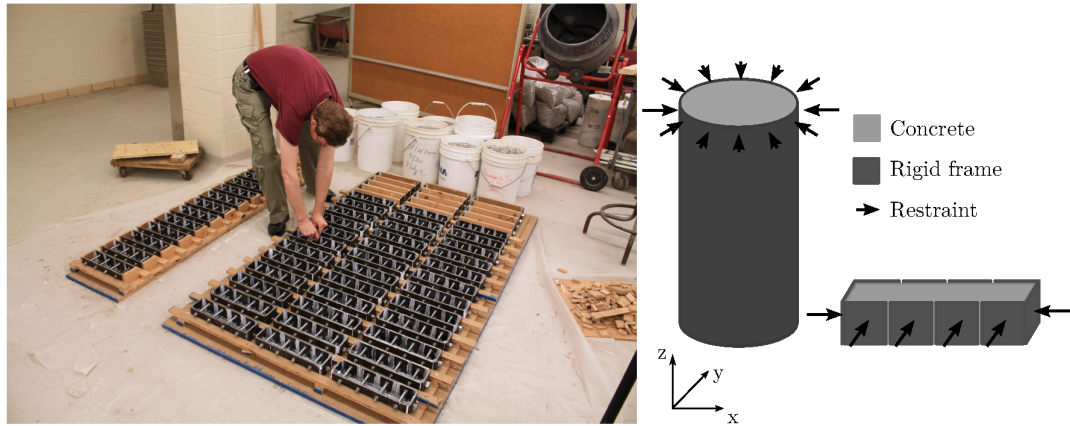


Figure 2: Formwork for the casting of the restrained samples (left). The setup usually used for restraint experiments is the cylinder setup. The prismatic setup presented in this paper allows different levels of restraint on the x and y axes.

Table 1: Restraint conditions tested.  $\delta$  is the difference in the stiffness of the restraining rods,  $\phi$  is their ratio.  $E_l$  is the stiffness of the lateral reinforcement,  $E_L$  the stiffness of the longitudinal reinforcement.

$E_l \setminus E_L$	0 GPa	6.54 GPa	10.23 GPa	14.73 GPa
0 GPa	$\delta = 0, \phi = 1$	$\delta = 6.54, \phi = \infty$	$\delta = 10.23, \phi = \infty$	$\delta = 14.73, \phi = \infty$
5.11 GPa	$\delta = 5.11, \phi = \infty$	$\delta = 1.41, \phi = 1.28$	$\delta = 5.12, \phi = 2.00$	$\delta = -9.62, \phi = 2.88$
26.18 GPa	$\delta = 26.18, \phi = \infty$	$\delta = 19.64, \phi = 0.25$	$\delta = -15.95, \phi = 0.39$	$\delta = -11.45, \phi = 0.56$
40.91 GPa	$\delta = 40.91, \phi = \infty$	$\delta = -34.37, \phi = 0.16$	$\delta = -30.68, \phi = 0.25$	$\delta = -26.18, \phi = 0.36$

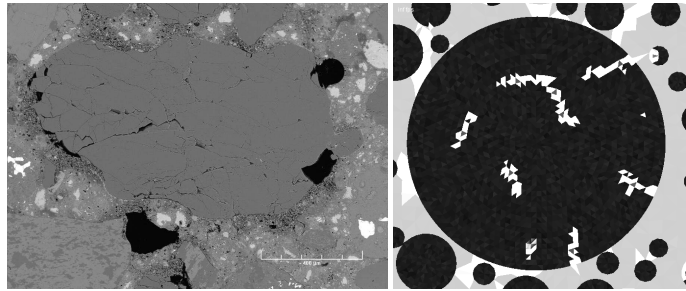


Figure 3: Back-scattered image of a reacted aggregate (left), simulation of a cracking aggregate (right). The nodes of the crack network are where the gel pockets are located.

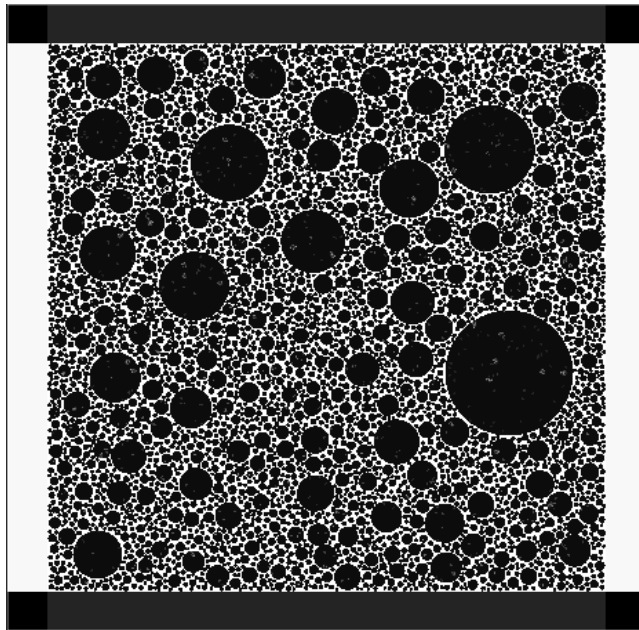


Figure 4: Simulated microstructure. The grey level indicates the relative stiffness of the materials, from black (stiffest) to white (softest).

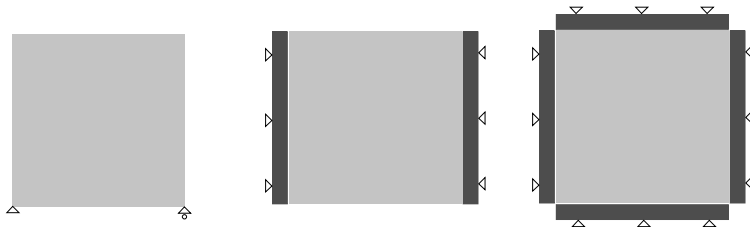


Figure 5: Boundary conditions used in the free, uni-axial restraint and bi-axial restraint cases.

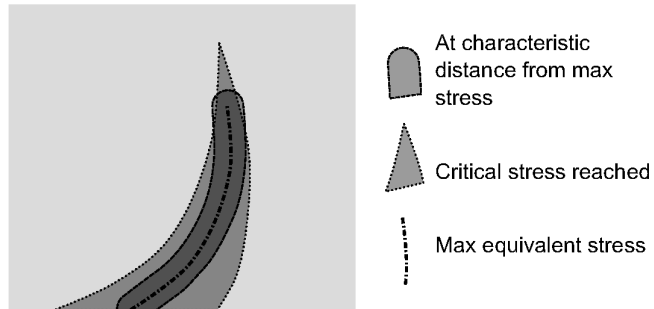


Figure 6: Locus considered to have reached its elastic limit (darker grey, all conditions met). The dotted line represents the peak max equivalent stress after an elastic evaluation. A configuration such as the one drawn on this figure could be observed near the tip of a micro-crack.

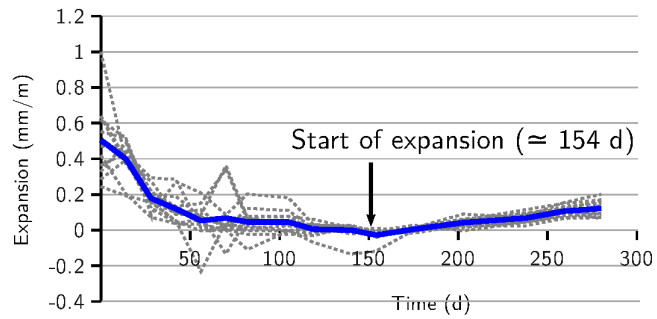


Figure 7: Lateral expansions to date.

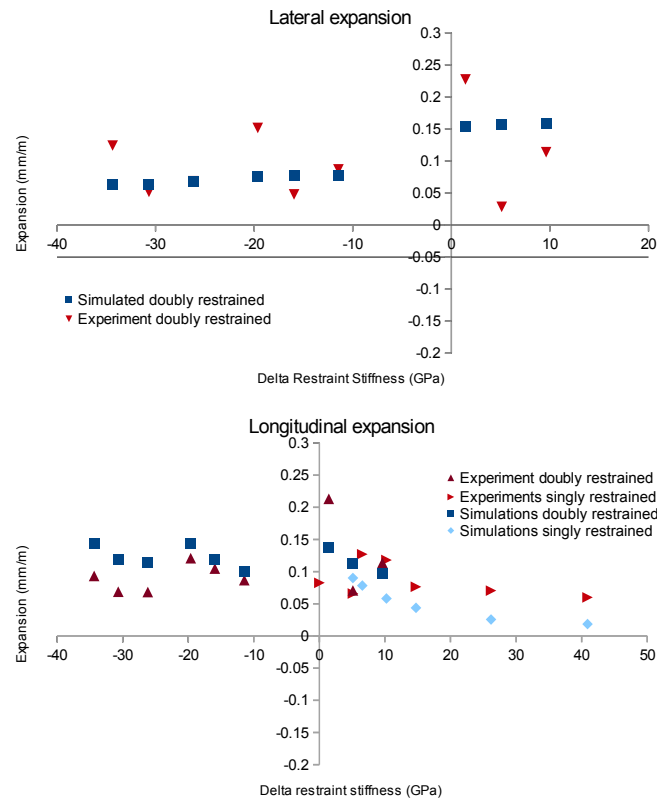


Figure 8: Compared experimental and simulated lateral and longitudinal expansions.

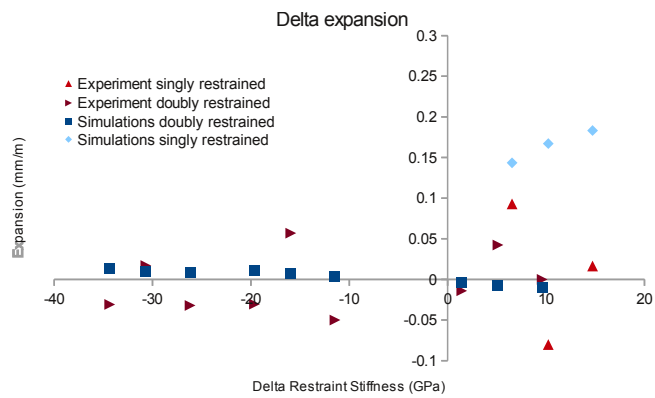


Figure 9: Compared experimental and simulated differences between lateral and longitudinal expansions.